



ELSEVIER

Colloids and Surfaces A: Physicochem. Eng. Aspects 219 (2003) 75–86

COLLOIDS  
AND  
SURFACES

A

www.elsevier.com/locate/colsurfa

# Intercalation of polymerization initiators into montmorillonite nanoparticle platelets: free radical vs. anionic initiator clays

Xiaowu Fan<sup>a</sup>, Chuanjun Xia<sup>a</sup>, Rigoberto C. Advincula<sup>a,b,\*</sup>

<sup>a</sup> *Materials Science Program, Department of Chemistry, University of Alabama at Birmingham, Birmingham, AL 35294-1240, USA*

<sup>b</sup> *Department of Chemistry, University of Houston, Houston, TX 77204, USA*

Received 8 August 2002; accepted 30 December 2002

## Abstract

We have investigated the properties of clay surface bound initiators for the preparation of polymer-layered silicate nanocomposite materials: one for anionic and two for free radical polymerization. These organic cations were intercalated into the galleries of montmorillonite clay by cation exchange. The structural, thermal, and compositional properties of the three types of initiator clays were studied and compared. X-ray diffraction studies showed that all three systems were swelled after initiator intercalation and the increase of interlayer d-spacing was dependent on the structure and molecular chain length of the initiators. Thermal gravimetric analysis, differential scanning calorimetry, and X-ray photoelectron spectroscopy traces indicated the presence of the initiator on clay and a complete cation exchange process was achieved only by adding excessive amounts of initiator. Infrared spectra compositionally confirmed the successful initiator intercalation into the clay platelets. Important differences were found between surface bound mono and dicationic free radical initiators.

© 2003 Elsevier Science B.V. All rights reserved.

*Keywords:* Montmorillonite; Intercalation; Ion exchange; Free radical polymerization initiator; Anionic polymerization initiator

## 1. Introduction

Polymer-layered silicate (PLS) nanocomposite materials have continuously attracted intensive and extensive interests since Toyota researchers first published their work on nylon 6-clay hybrid materials in the late 80s and early 90s [1]. Recently, other PLS composite materials such as polyimide,

[2] epoxy resin [3,4], polystyrene, [5–7] polycaprolactone, [8] polypropylene, [9] polyvinyl alcohol, [10] and polyurethane [11] have been reported. The interest in PLS nanocomposites is practically attributed to their improved mechanical, barrier, and heat-resistant properties over their pristine macro-composite counterparts. Furthermore, layered clays, such as montmorillonite aluminosilicates, possess exchangeable metal cations ( $\text{Na}^+$ ,  $\text{Li}^+$ ,  $\text{Ca}^{2+}$ , etc.) at the spacing between layers. As a result, various organic cations can be inserted into the interlayer galleries by an ion exchange process, forming an inorganic clay–organic mole-

\* Corresponding author. Tel.: +1-7137431760; fax: +1-7137432709.

E-mail address: [radvincula@uh.edu](mailto:radvincula@uh.edu) (R.C. Advincula).

cule complex, i.e. organically-modified layered silicate (OLS). As a class of materials, they are ideal systems to study theories related to interface science and intercalation thermodynamics of organic species in confined and tethered environments [12].

From a structural standpoint, there are two types of PLS nanocomposites: [13] (1) *Intercalated*: the polymer chains are inserted into the interlayer spacing of the stacking silicate platelets. The d-spacing value of this well-ordered, polymer-silicate sandwich multilayer is greater than that of pristine clay. (2) *Delaminated/exfoliated*: the clay layers are individually and randomly dispersed in a continuous polymer matrix. Because of greater phase homogeneity of the latter, the delaminated structure is more effective in improving the properties of a material, especially at very low silicate loading. Thus, a delaminated structure is more desirable than an intercalated one in terms of composite material synthesis.

To obtain a delaminated/exfoliated structure, two methods are usually followed: (1) intercalation of a suitable monomer and subsequent intercalative polymerization. (2) Intercalation of a suitable initiator and subsequent in situ surface initiated polymerization (SIP). The significance of in situ SIP lies in a sound assumption that, as the polymer chain grows, the ordered silicate layers would be gradually pushed apart, ultimately exfoliating to discrete sheets. This results in a well-dispersed structure of the final product. Although the first method has been used throughout the history of PLS nanocomposite preparation, it has limited application because of poor miscibility between organophobic clay and most monomers. Furthermore, a monomer suitable for intercalation is not always available for most of the technologically important polymers [14]. Recently, it was reported that delaminated, molecular weight (MW) controllable nanocomposites could be successfully synthesized by anchoring a living free radical polymerization initiator into the galleries of layered silicate with subsequent in situ polymerization [7].

From the preceding introduction, it is clear that intercalation of initiators into the intergalleries of clay is a very important step towards a delami-

nated nanocomposite structure. It plays a very crucial role in the whole synthetic scheme. First of all, the inserted molecules provide initiation functionalities for polymerization. Second, the surface tethered organic initiator improves organophilicity of the silicate clay, which can facilitate homogeneity of the initiator clay–monomer–organic solvent system.

In our efforts to conduct SIP on clay, we recently synthesized three initiators for free radical and anionic polymerization. All of them have a quaternized amine end-group that allows cation exchange with montmorillonite clay. The initiator molecule design is as follows: symmetric, with two cationic groups at both chain ends (named difunctional free radical initiator hereafter) and asymmetric, with one cationic group at one end (named monofunctional free radical initiator hereafter). These are AIBN-analogue initiators that can initiate free radical polymerization. The third initiator is a diphenylethylene (DPE) derivative capable of initiating anionic polymerization (named anionic initiator hereafter). The synthetic schemes and structures of these initiators are shown in Fig. 1(a–c). The chain length values (estimated after MM2 energy minimization by CHEM-3D software) for those molecules are also shown. Recently, we have reported our initial results on living anionic SIP (LASIP) from clay surfaces by polymerizing the clay intercalated with the DPE derivative [15–17]. We have also used the monofunctional free radical initiator to graft polymer brushes from clay surfaces on planar substrates [18]. Comparative studies on the different effects of mono- and difunctional initiators on free radical SIPs from clay nanoparticles are underway [19].

Other cationic initiators have been employed to synthesize the PLS nanocomposite materials by other researchers [20,21]. However their emphasis was primarily on properties of the final products. The intercalated intermediates were not very well characterized and the results of initiator intercalation were not reported in detail. In this paper, we hereby report our detailed comparative studies on the intercalation of these initiators into montmorillonite clay with regards to their structural, thermal and compositional properties.

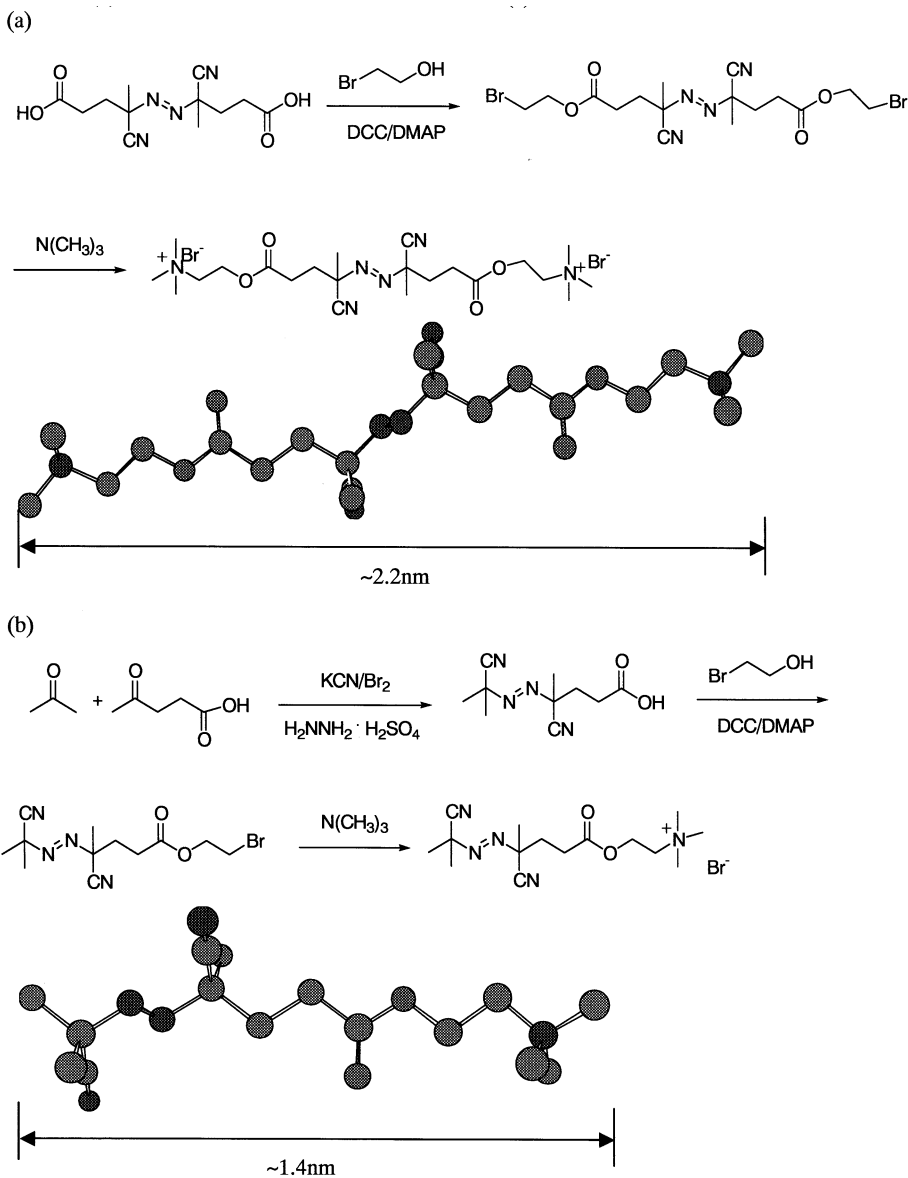


Fig. 1. Synthetic schemes and structures of the initiators: (a) difunctional free radical initiator, (b) monofunctional free radical initiator, and (c) anionic initiator.

## 2. Experimental

### 2.1. Materials

Montmorillonite clay (commercially Cloisite<sup>®</sup> Na<sup>+</sup>) was donated by Southern Clay Products

Inc. Deionized water used in all experiments was purified by a Milli-Q Academic<sup>®</sup> system (Millipore Cooperation) with a 0.22 micron Millistack filter at the outlet. All reagents for the synthesis of the initiators were commercially available and used without further purification.

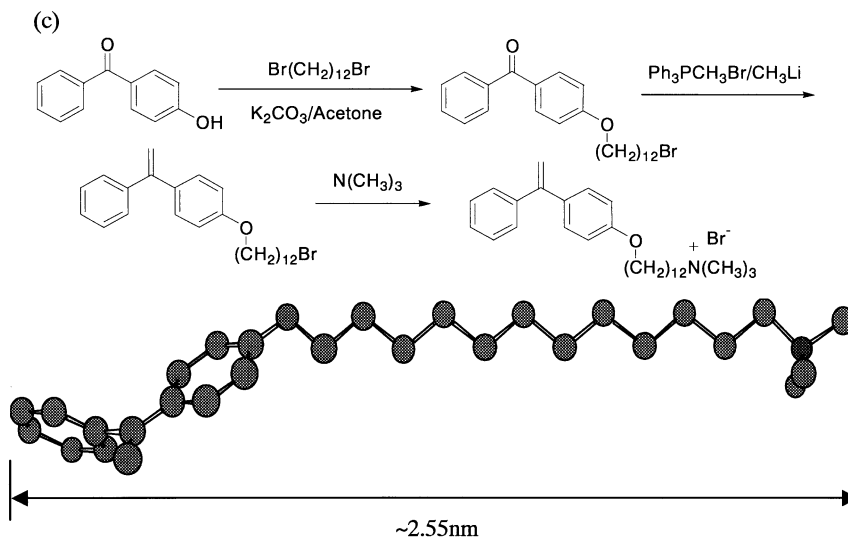


Fig. 1 (Continued)

## 2.2. Initiator synthesis

The synthesis routes of the three initiators are shown in Fig. 1(a–c). The synthesis of the symmetric radical initiator started from the commercially available 4,4'-azobis(4-cyanovaleric acid), which was purchased from Acros. The acid was treated with bromoethanol by a well-known esterification method using DCC/DMAP [22], followed by stirring with excess trimethylamine in anhydrous THF. The precipitate was collected and dried under vacuum as the final product. The asymmetric initiator was made in a similar way except that the starting material was synthesized differently as reported [23]. As shown in Fig. 1(c), 1,1-DPE was rendered cationic by functionalizing with a trimethyl ammonium bromide group. The 3-hydroxybenzophenone was first reacted with 1,12-dibromododecane to form an ether linkage followed by a Wittig reaction to convert the ketone into an ethylene functional group. Quaternization of the terminal  $-\text{CH}_2-\text{Br}$  functionality with trimethyl amine resulted in the final product (trimethyl-12-[4-(1-phenyl-vinyl)-phenoxy]-dodecyl}-ammonium bromide). Details of the initiator synthesis have been reported elsewhere [16,18].

## 2.3. Preparation of initiator clay

A certain amount of montmorillonite clay (Table 1) was dispersed in 500 ml deionized water and the dispersion was stirred vigorously overnight at room temperature. The clay suspension was then ultrasonicated while stirring for 24 h and a yellowish, homogenous dispersion was obtained. All three initiators were dissolved in deionized water to make 1.25 wt.% aqueous solution. By using the cation exchange capacity (CEC) value (92 mequiv/100 g) of the Cloisite  $\text{Na}^+$  and the MW of different initiators, the exact weight (the weight of the initiator needed to fully replace the sodium counter ion of the clay used) of the three initiators was calculated. Accordingly, an excess amount of initiator solution was slowly poured into the clay dispersion while it was being stirred and ultrasonicated. The mixture was stirred for another 24 h. The resulting white precipitate was separated by filtration and then re-dispersed in deionized water. This filtration-dispersion process was repeated 10 times in order to remove the free, unattached initiator. Final products were weighed after drying the precipitates in a vacuum oven for 3 days and the yield percentage was calculated.

Table 1  
Data related with the preparation of initiator clays

Initiator	Clay used (g)	Theoretical initiator weight (g)	Initiator actually added (g)	Initiator clay obtained (g)	Yield (%)
Difunctional free radical	1.3	0.366	0.45	1.35	87.5
Monofunctional free radical	1.3	0.464	0.625	1.47	89.6
Anionic	1	0.462	0.516	1.20	87.8

Table 1 summarizes the data concerning the fabrication of the three types of initiator clays. The yellowish powder products were stored in a desiccator for further characterization and subsequent SIPs.

## 2.4. Characterization

### 2.4.1. X-ray diffraction

X-ray diffraction (XRD) analysis of clay powder samples were performed on a Philips X'pert PW3040-MPD model diffractometer with a Cu-K $\alpha$  incident beam of wavelength 0.1543 nm. The Bragg equation was applied to calculate the d-spacing of the clay platelets.

### 2.4.2. Thermal analysis

Thermogravimetric analysis (TGA) and differential scanning calorimetry (DSC) were performed on a combined model of Mettler DSC30 and TGA50 with a heating rate of 10 °C min<sup>-1</sup> for DSC and 20 °C min<sup>-1</sup> for TGA. All measurements were performed under nitrogen flow. The samples were in powder state and dried in vacuum oven at room temperature for at least 24 h to remove moisture before the measurements.

### 2.4.3. Infrared spectroscopy

Infrared spectra were obtained on a Nicolet NEXUS 470 FT-IR system. Powder samples were dispersed in anhydrous methylene chloride and drops of the liquid were spread on KBr plates. All sample discs were fully dried by air flow before analysis. The spectra were scanned 64 times with a resolution of 4 cm<sup>-1</sup>.

### 2.4.4. X-ray photoelectron spectroscopy

Powder samples of pure and initiator clays were analyzed by a Kratos Axis 165 Multitechnique Electron Spectrometer system. Powder samples were first pressed onto double-sided carbon tape before loading into the X-ray photoelectron spectroscopy (XPS) analysis chamber. A non-monochromatic Al-K $\alpha$  X-ray source (1486.6 eV) operated at 15 kV and 20 mA was applied to excite the photoelectron emission. Fixed analyzer transmission mode was used and survey scans (spot 800 × 200  $\mu\text{m}^2$ , resolution 4 eV at analyzer pass energy of 160 eV) were collected from 0 to 1400 eV to obtain elemental composition of the powder samples. C 1s peak of hydrocarbon signal (284.5 eV) was used as binding energy reference. A built-in charge neutralizer was operated to compensate for charge build-up during the measurements.

## 3. Results and discussion

X-ray powder diffraction patterns of the pristine clay and the three intercalated clay samples are shown in Fig. 2. By using the Bragg equation,  $n\lambda = 2d\sin\theta$ , the d-spacing values of the samples were calculated and shown beside each peak.

The basal spacing of pure montmorillonite-Na<sup>+</sup> is 1.16 nm, which is in accordance with data from other sources [24]. Obviously, these XRD patterns indicate the successful intercalation of the initiator molecules into the galleries of silicate platelets since all three initiator clay samples gave increased d-spacing values. Also, the increased diffraction intensity provides more evidence of a well-ordered swollen structure after intercalation. This result

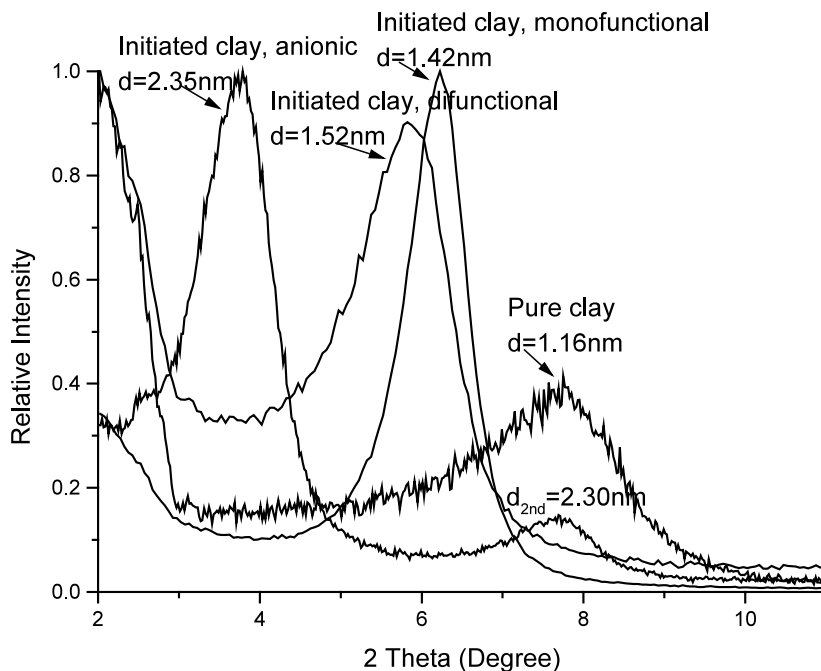


Fig. 2. X-ray powder diffraction patterns of pure clay and 3 initiator clay samples.

demonstrates that the layered framework of inorganic clay can accommodate our organic initiators with various functionalities with better long-range special periodicity. Noticeably, the increasing sequence of d-spacing values is consistent with the steric sizes (Fig. 1(a–c)) of the initiator molecules, i.e., the longer molecule (anionic initiator) gave larger d-spacing while the shorter molecule (monofunctional free radical initiator) gave smaller d-spacing. Although the chain length (2.2 nm) of difunctional free radical initiator is much larger than the monofunctional one (1.4 nm), the d-spacing of the former is slightly more (0.1 nm) than the latter. The reason for this observation lies in the presence of charged groups on both ends of the molecule. Thus, there are mainly two intercalation possibilities: the two cationic end groups electrostatically interact with two different but neighboring platelets' surfaces or they attach to the same side of one clay particle. The combination of these two possibilities make the intercalated structure less spatially-ordered which could account for the significantly broad peak for this sample as compared with those of the

other two initiator clay samples (Fig. 2). Furthermore, since XRD collects average information from a large area of a powder sample, a synergistic effect of these two possibilities are shown by having a d-spacing value in between. The above interpretation is schematically shown in Fig. 3. The interlamellar height value shown in the figure is calculated by:  $\Delta d = d\text{-spacing} - \text{thickness of one platelet} (\sim 0.9 \text{ nm})$ .

In the case of the clay intercalated with anionic initiator, the distance between two adjacent clay platelets is 1.45 nm. Another study showed a very close 1.43 nm gallery height of the intercalated montmorillonite by a molecule with a  $C_{18}H_{37}$  alkyl tail and a quaternized amine end [25]. Its chain length value was also estimated by CHEM-3D software to be 2.41 nm, indicating the consistency of the results in terms of the intercalated molecules' dimensions.

Interestingly, for the anionic initiator clay, another small intensity peak was observed at  $2\theta = 7.7^\circ$  besides the high intensity peak at  $2\theta = 3.8^\circ$ . There are two possibilities for this secondary peak. (1) It might be a second-order diffraction

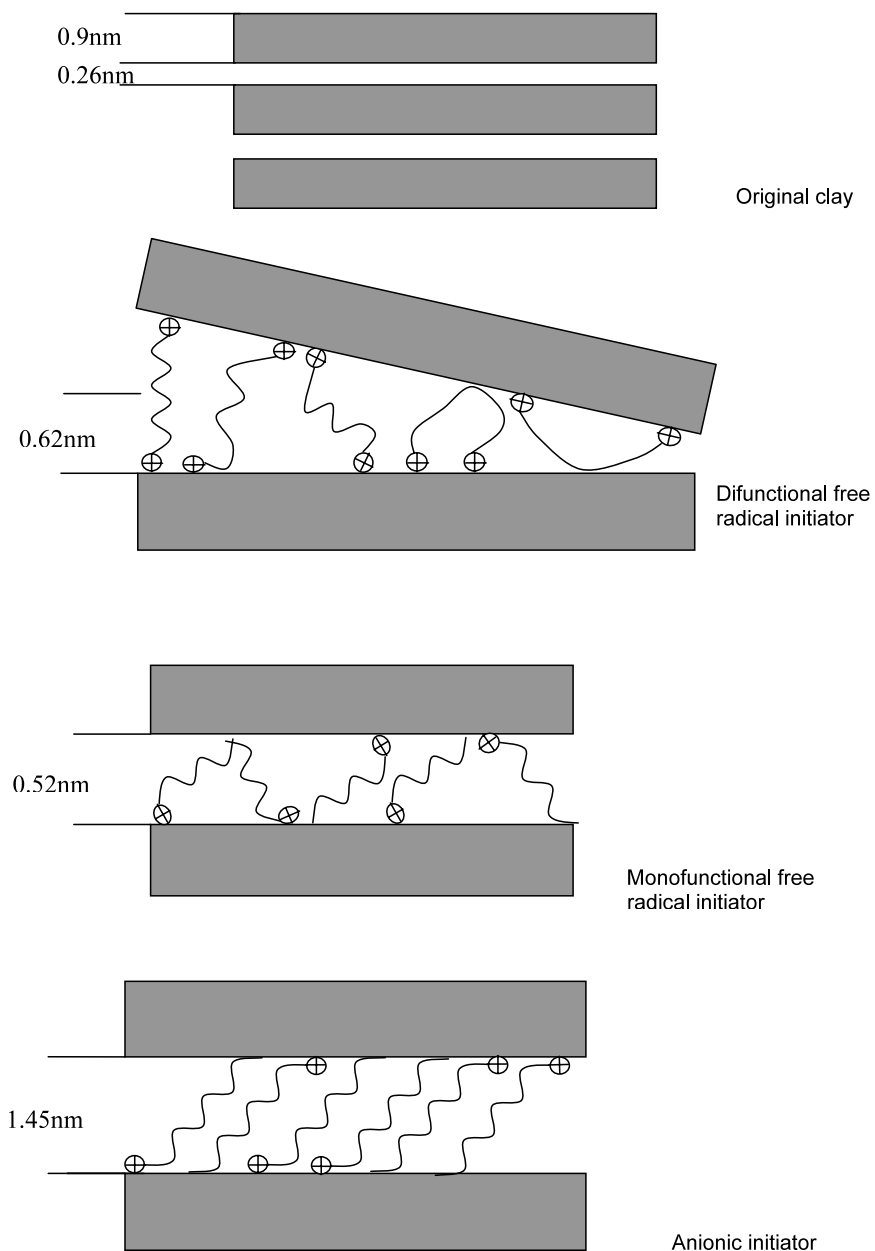


Fig. 3. Schematics of different intercalations.

peak from (0 0 2) planes and the basal spacing is calculated to be 2.3 nm, which is very close to the value of its first-order diffraction peak. Similar higher order diffraction peaks (up to the third order) were also observed for intercalated smectite clays [26]. (2) Because the position of this peak

coincides with that of the peak of the pristine clay, it might also originate from the remaining, unswollen clay particles, which are not intercalated with the initiator. However, it should be noted that the second possibility could be ruled out by TGA, DSC, and XPS results (see below).

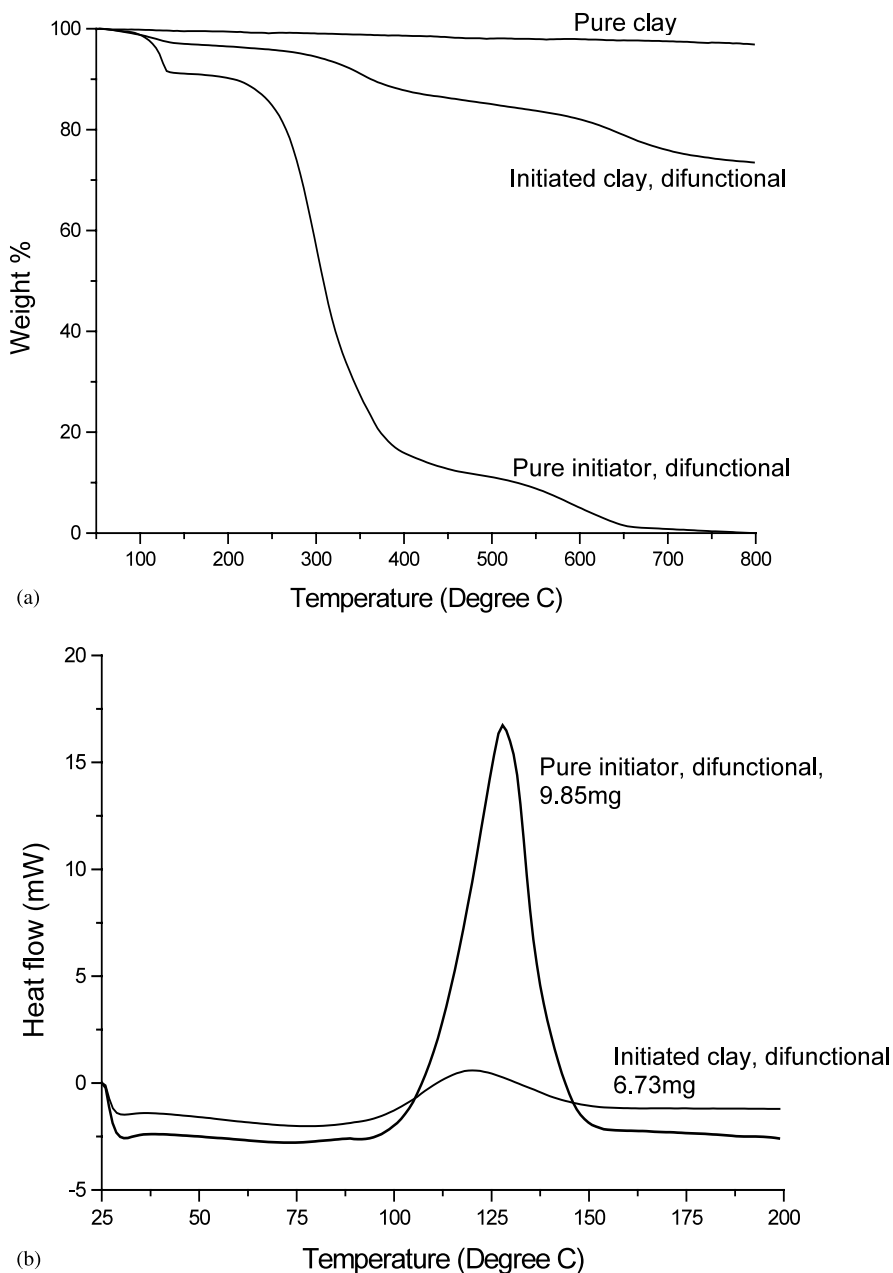


Fig. 4. Thermal properties of pure clay, clay intercalated with difunctional initiator, and pure difunctional initiator: (a) TGA traces and (b) DSC traces.

Thermal properties of these three OLS systems were studied by TGA and DSC. Fig. 4(a) shows the TGA traces of pure clay, clay intercalated with difunctional initiator, and pure initiator. As could be expected, the inorganic montmorillonite silicate

shows a high thermal stability. The total weight loss is only 3.1% up to 800 °C. This small percentage of weight loss is due to 3 different types of water present in the montmorillonite clay [27]. On the contrary, the organic initiator totally



decomposes over the experimental temperature range. On the curve of the pure initiator, there is a dramatic weight loss at about 120 °C, indicating the decomposition of the azo group and the evolution of N<sub>2</sub>. Also for the initiated clay, this decomposition occurs at the same temperature range and the overall degradation behavior is quite similar to that of the pure initiator, which shows the initiator is attached to the clay particle.

The montmorillonite clay we used has a CEC value of 92 mequiv/100 g. According to this value, the ideal organic weight percentage of difunctional initiated clay is calculated to be 17.5%. However, the corresponding TGA weight loss for the initiated clay sample is 23.8% (total weight loss—weight loss of pure clay), which is greater than the calculated value. One possibility for this difference is that an excessive amount of initiator was added and the free unattached initiator was not totally washed away. Nevertheless, excess amount of initiator was necessary in order to achieve a complete cation exchange and intercalation process in clay. Similar procedures for the total replacement of exchangeable cations on clay were also emphasized by other researchers [7].

Besides TGA, the thermal behavior of the pure initiator and initiated clays was further investi-

gated by DSC. The percentage of initiator in the initiated clay is also calculated by the enthalpy change of the azo group decomposition. As can be seen from Fig. 4(b), both samples exhibited exothermic behavior at 100–150 °C. The total energy released was calculated by integrating the peak area. The enthalpy/weight ratio was obtained by dividing the integration by individual sample weight. The results showed 60.97 J g<sup>-1</sup> for the difunctional initiator clay and 240.39 J g<sup>-1</sup> for pure difunctional initiator. Thus the weight percentage of the initiator in the OLS clay was calculated to be 25.4%, which is consistent with the TGA weight loss. Both thermal analyses confirmed the completion of the cation exchange process.

Similar TGA and DSC measurements were performed on the samples associated with the monofunctional free radical initiator and similar quantitative results were obtained. As compared to the ideal initiator weight percentage 22.5% from the CEC value, the actual TGA weight loss is 28.5% and the weight percentage is 30.4% from DSC enthalpy change. The results are consistent with those of the difunctional initiator clay.

Fig. 5 shows the TGA results of pure clay, pure anionic initiator and anionic initiator clay. From

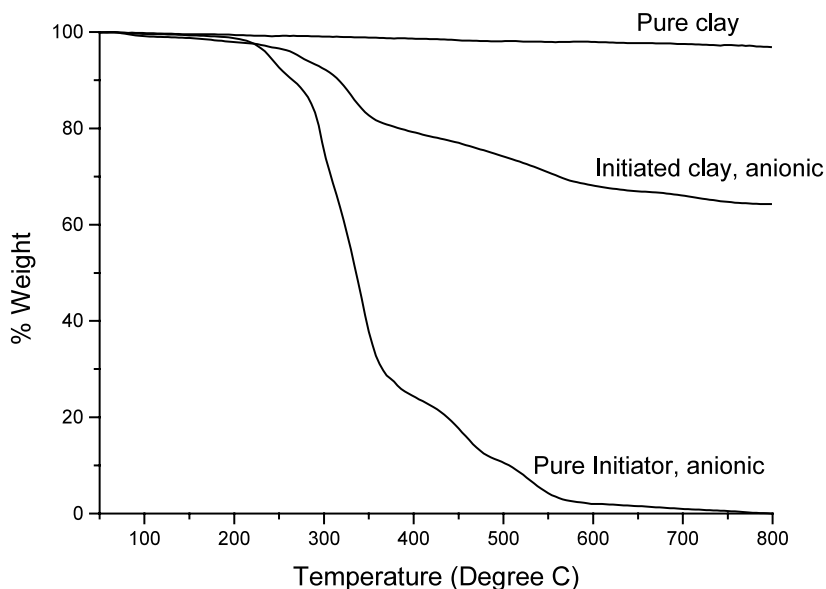


Fig. 5. TGA traces of pure clay, clay intercalated with anionic initiator, and pure anionic initiator.

the curves, it is clear that the pure initiator and the initiator clay have very similar thermal decomposition behavior. They both exhibit a two-step decomposition process: one major weight loss at the temperature range of approximately 250–350 °C and a minor weight loss at about 350–600 °C. The low temperature degradation is due to breakdown of the DPE unit while the high temperature degradation is consistent with decomposition of the alkyl spacer. This clearly proves the attachment of the organic initiator to the inorganic clay surface. Also, the same calculation was done using the CEC value: the ideal organic weight percentage for the anionic initiator clay is 28.4% and the TGA weight loss is 32.6%. Their consistency again indicates the completion of the cation exchange for this batch of clay samples. On the other hand, a small portion of free, unattached initiator was not totally washed away.

IR analysis further confirmed the existence of organic initiators on the intercalated clay samples. In Fig. 6, the IR spectrum of pure clay only shows strong absorbance at  $1040\text{ cm}^{-1}$  due to the Si–O bond in montmorillonite silicate. The spectrum of pure anionic initiator shows its strong characteristic peaks at  $3100\text{--}2800\text{ cm}^{-1}$  due to aromatic and aliphatic C–H stretching,  $1475\text{--}1300\text{ cm}^{-1}$  due to alkyl C–H bending,  $1675\text{--}1550\text{ cm}^{-1}$  due to aromatic and aliphatic C=C stretching. Also, peaks within the range of  $1520\text{--}1480\text{ cm}^{-1}$  can be attributed to C–N bond deformation and peaks near  $1250\text{ cm}^{-1}$  are the result of alkyl C–C stretching. The above peaks in the spectra of pure silicate and pure initiator can be easily found in the same spectral region of initiator clay. It is apparent that a synergistic effect is observed from the previous two spectra, which clearly demonstrates attachment of the initiator on clay surface. Similar IR results of this synergistic effect on other OLS' were observed in polyaniline-montmorillonite and styrene-acrylonitrile-montmorillonite systems [28,29]. Fig. 6 also show the spectra of the two free radical initiators. As expected, the spectra of the two pure initiators also show the characteristic absorption peaks of C–H bond at  $2950\text{--}2800\text{ cm}^{-1}$ , C=O (carbonyl) bond at  $1734\text{ cm}^{-1}$ , and C≡N (nitrile) bond at  $2243\text{ cm}^{-1}$ . Very similarly, the corresponding spectra of the two initiator

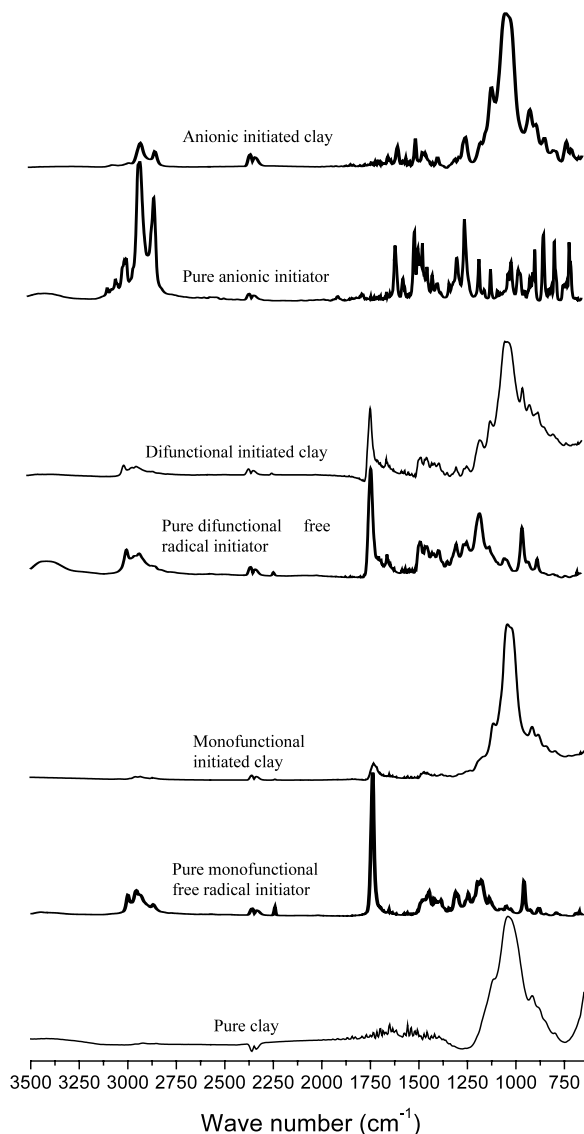
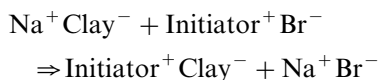


Fig. 6. IR spectra of pure clay, pure initiators, and initiator clays.

(monofunctional and difunctional) clay samples show the same low intensity but discernable peaks. Although the IR absorbance for initiator clay samples is quite low, the attachment of initiators on the clay surface is still affirmative.

The cation exchange process between the montmorillonite and  $\text{Na}^+$  clay and the charged initiator can be simplified by the following reaction:



By using XPS, the completion of the above ion exchange reaction was further confirmed. Fig. 7 show the XPS survey scan spectra of the pure and initiator clay samples. As labeled in curve (a), characteristic peaks of O, Si, Al, Mg are very clear for the pristine montmorillonite clay, which is chemically magnesium aluminum silicate. Besides these signals from the clay, curves (b–d) also show C 1s and N 1s peaks, again demonstrating the presence of the organic initiator molecules on the clay. However, the most important result from XPS analysis is the change in Na signal before and after the ion exchange reaction. As indicated in the spectrum of pure clay, the photoelectron line of Na 1s (1072 eV) and Auger line of Na KLL (493 eV) are very obvious, indicating that the clay's counter ion is Na cation. After cation replacement, those two characteristic emissions for Na disappear for all three initiator clay samples. This provides more evidence to support a complete cation exchange process. Moreover, it is clear that

the second XRD peak previously shown should be a second order diffraction of totally swelled clay lamella, rather than a signal from a remnant portion of unintercalated clay particles.

#### 4. Conclusions

Three charged initiators, one for LASIP and the other two for free radical SIP, were successfully synthesized and characterized. Their properties of intercalation into montmorillonite clay were comparatively analyzed. XRD results showed that the d-spacing increase of intercalated clay stacking was dependent on the structure and functionality of different initiators. The difunctional is less ideally packed than the monofunctional. Nevertheless, IR, XPS, and qualitative TGA and DSC confirmed the attachment of the initiator. Complete replacement of the clay counter ion by charged initiators was demonstrated quantitatively by TGA, DSC, and XPS. Above all, a simple stirring-ultrasonicating process at room temperature allowed successful intercalation and complete

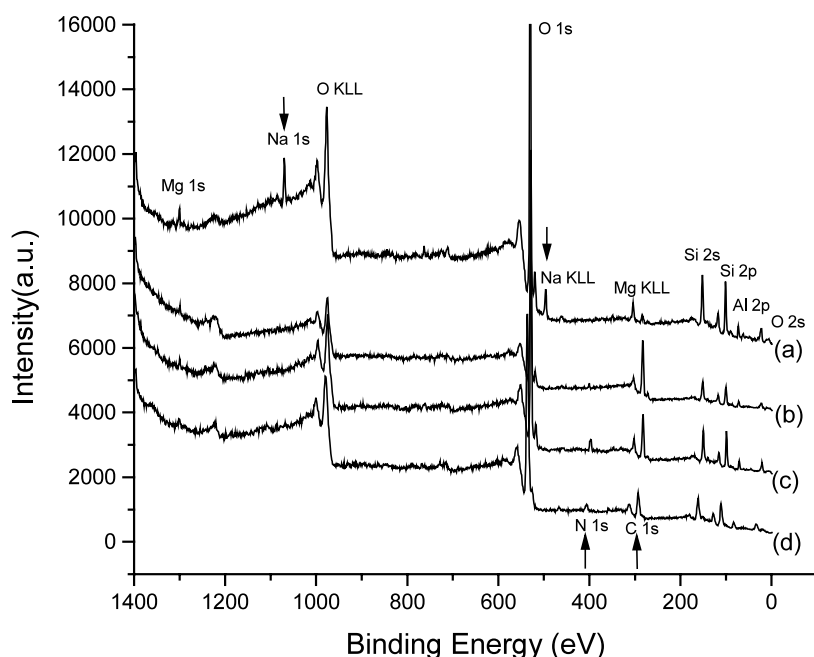


Fig. 7. XPS spectra of pure clay and 3 initiator clay samples: (a) pure clay, (b) difunctional initiated clay, (c) monofunctional initiated clay, and (d) anionic initiated clay.

ion exchange with montmorillonite clay. These results confirmed the successful use of these initiator clays for SIP both by free radical and anionic mechanisms.

### Acknowledgements

This project is supported by the Army Research Office (Grant number: DAAD-19-99-1-0106). Montmorillonite clay (commercially Cloisite Na<sup>+</sup>) is generously donated by Southern Clay Product, Gonzales, TX. We would like to thank other co-workers who had previously contributed to the project, Qingye Zhou, Walter Cristofoli, and Professor Jimmy Mays (University of Tennessee-Knoxville). We also appreciate Dr Yogesh Vohra and Dr Shane Cetledge, Dr Juan Pablo Claude, and John Kestell at University of Alabama at Birmingham for their help on XRD and IR analysis. We also acknowledge Dr Earl Ada at University of Alabama-Tuscaloosa for XPS measurements.

### References

- [1] (a) A. Usuki, Y. Kojima, M. Kawasumi, A. Okada, T. Kurauchi, O. Kamigaito, *Polym. Prepr.* 31 (1990) 651; (b) A. Okada, M. Kawasumi, T. Kurauchi, O. Kamigaito, *Polym. Prepr.* 28 (1987) 447; (c) A. Usuki, Y. Kojima, M. Kawasumi, A. Okada, Y. Fukushima, T. Kurauchi, O. Kamigaito, *J. Mater. Res.* 8 (1993) 1179; (d) Y. Kojima, A. Usuki, M. Kawasumi, A. Okada, Y. Fukushima, T. Kurauchi, O. Kamigaito, *J. Mater. Res.* 8 (1993) 1185; (e) Y. Kojima, A. Usuki, M. Kawasumi, A. Okada, T. Kurauchi, O. Kamigaito, *J. Polym. Sci., Part A: Polym. Chem.* 31 (1993) 983; (f) Y. Kojima, A. Usuki, M. Kawasumi, A. Okada, T. Kurauchi, O. Kamigaito, *J. Polym. Sci., Part A: Polym. Chem.* 31 (1993) 1755.
- [2] K. Yano, A. Usuki, A. Okada, T. Kurauchi, O. Kamigaito, *J. Polym. Sci., Part A: Polym. Chem.* 31 (1993) 2493.
- [3] T. Lan, T.J. Pinnavaia, *Chem. Mater.* 6 (1994) 2216.
- [4] M.S. Wang, T.J. Pinnavaia, *Chem. Mater.* 6 (1994) 468.
- [5] R.A. Vaia, H. Isii, E.P. Giannelis, *Chem. Mater.* 5 (1993) 1694.
- [6] A. Akelah, A. Moet, *J. Mater. Sci.* 31 (1996) 3589.
- [7] M.W. Weimer, H. Chen, E.P. Giannelis, D.Y. Sogah, *J. Am. Chem. Soc.* 121 (1999) 1615.
- [8] P.B. Messersmith, E.P. Giannelis, *J. Polym. Sci., Part A: Polym. Chem.* 33 (1995) 1047.
- [9] M. Kawasumi, N. Hasegawa, A. Musuki, A. Okada, *Macromolecules* 30 (1997) 6333.
- [10] K.E. Strawhecker, E. Manias, *Chem. Mater.* 12 (2000) 2943.
- [11] Z. Wang, T.J. Pinnavaia, *Chem. Mater.* 10 (1998) 3769.
- [12] (a) E.P. Giannelis, R. Krishnamoorti, E. Manias, *Advances Polym. Sci.* 138 (1999) 107; (b) R. Krishnamoorti, R.A. Vaia, E.P. Giannelis, *Chem. Mater.* 8 (1996) 1728; (c) S. Park, A. Fitch, Y. Wang, *Phys. Chem.* 13 (1997) 4889; (d) A.C. Balazs, C. Singh, E. Zhulina, Y. Lyatskaya, *Acc. Chem. Res.* 32 (1999) 651.
- [13] S.D. Burnside, E.P. Giannelis, *Chem. Mater.* 7 (1995) 1597.
- [14] E.P. Giannelis, *Adv. Mater.* 8 (1996) 29.
- [15] Q. Zhou, X. Fan, C. Xia, J. Mays, R.C. Advincula, *Chem. Mater.* 13 (2001) 2465.
- [16] X. Fan, Q. Zhou, C. Xia, W. Cristofoli, J. Mays, R.C. Advincula, *Langmuir* 18 (2002) 4511.
- [17] X. Fan, C. Xia, W. Cristofoli, Q. Zhou, J. Mays, R.C. Advincula, *Polym. Prepr.* 43 (2002) 682.
- [18] X. Fan, C. Xia, T. Fulghum, M.K. Park, J. Locklin, R.C. Advincula, *Langmuir* 19 (2003) 916.
- [19] X. Fan, C. Xia, R.C. Advincula, *Langmuir* (submitted for publication).
- [20] L.P. Meier, R.A. Shelden, W.R. Caseri, U.W. Suter, *Macromolecules* 27 (1994) 1637.
- [21] C. Zilg, R. Thomann, M. Baumert, J. Finter, R. Mulhaupt, *Macromol. Rapid Commun.* 21 (2000) 1214.
- [22] B. Neises, W. Steglich, *Angew. Chem. Int. Ed.* 17 (1978) 522.
- [23] O. Prütcker, J. Rühle, *Macromolecules* 31 (1998) 592.
- [24] N.A. Kotov, T. Haraszti, L. Turi, G. Zavala, R.E. Geer, I. Dekany, J.H. Fendler, *J. Am. Chem. Soc.* 119 (1997) 6821.
- [25] R.A. Vaia, R.K. Teukolsky, E.P. Giannelis, *Chem. Mater.* 6 (1994) 1017.
- [26] M. Okamoto, S. Morita, H. Taguchi, H. Kim, T. Kotaka, H. Tateyama, *Polymer* 41 (2000) 3887.
- [27] W. Xie, Z. Gao, W. Pan, D. Hunter, R.A. Vaia, A. Singh, *PMSE Prepr.* 82 (2000) 284.
- [28] H.J. Choi, J.W. Kim, S.G. Kim, B.H. Kim, J. Joo, *PMSE Prepr.* 82 (2000) 245.
- [29] H.J. Choi, J.W. Kim, M.S. Jhon, *PMSE Prepr.* 82 (2000) 247.